Numerical Heat Transfer, Part A: Applications: An International Journal of Computation and Methodology
Publication details, including instructions for authors and subscription information:
http://www.tandfonline.com/loi/unht20

Natural Convection in Differentially Heated Partially Porous Layered Cavities Filled with a Nanofluid

Ali J. Chamkha [a] & Muneer A. Ismael [b]
[a] Manufacturing Engineering Department , The Public Authority for Applied Education and Training , Shuweikh , Kuwait
[b] Mechanical Engineering Department , Engineering College, University of Basrah , Basrah , Iraq
Published online: 17 Mar 2014.

To cite this article: Ali J. Chamkha & Muneer A. Ismael (2014) Natural Convection in Differentially Heated Partially Porous Layered Cavities Filled with a Nanofluid, Numerical Heat Transfer, Part A: Applications: An International Journal of Computation and Methodology, 65:11, 1089-1113, DOI: 10.1080/10407782.2013.851560

To link to this article: http://dx.doi.org/10.1080/10407782.2013.851560

Numerical Heat Transfer, Part A, 65: 1089–1113, 2014

ISSN: 1040-7782 print/1521-0634 online
DOI: 10.1080/10407782.2013.851560

Taylor & Francis
Taylor & Francis Group

NATURAL CONVECTION IN DIFFERENTIALLY HEATED PARTIALLY POROUS LAYERED CAVITIES FILLED WITH A NANOFLUID

Ali J. Chamkha[1] and Muneer A. Ismael[2]

[1]*Manufacturing Engineering Department, The Public Authority for Applied Education and Training, Shuweikh, Kuwait*

[2]*Mechanical Engineering Department, Engineering College, University of Basrah, Basrah, Iraq*

Natural convection heat transfer in a differentially heated and vertically partially layered porous cavity filled with a nanofluid is studied numerically based on double–domain formulation. The left wall, which is adjacent to the porous layer, is isothermally heated, while the right wall is isothermally cooled. The top and bottom walls of the cavity are thermally insulated. Impermeable cavity walls are considered except the interface between the porous layer and the nanofluid layer. The Darcy–Brinkman model is invoked for the porous layer which is saturated with the same nanofluid. Equations govern the conservation of mass, momentum, and energy with the entity of nanoparticles in the fluid filling the cavity and that are saturated in the porous layer are modeled and solved numerically using under successive relaxation upwind finite difference scheme. The contribution of five parameters are studied, these are; nanoparticle volume fraction φ ***(0–0.1), porous layer thickness*** $\mathbf{Xp}$ ***(0–0.9), Darcy number*** $\mathbf{Da}$ ***(10^{-7}–1), aspect ratio*** $\mathbf{A}$ ***(1, 2, 4), and Rayleigh number Ra (10^3–10^6). The nanofluid is considered to be composed of copper nanoparticles and water as a base fluid. The results have shown that with the aid of a nanofluid, the convective heat transfer can be enhanced even at a low permeable porous medium. It is found that when*** $\mathbf{Ra} \leq 10^5$***, there is a critical porous layer thickness*** $\mathbf{Xp}$ ***at which the Nusselt number is maximum. Otherwise, the Nusselt number*** $\mathbf{Nu}$ ***decreases rapidly with*** $\mathbf{Xp}$***. Correlations of*** $\mathbf{Nu}$ ***with the other parameters are established and tested for*** $\mathbf{A} = 2$***.***

1. INTRODUCTION

The problem of a confined cavity partly filled with a fluid layer and partly with a porous layer saturated by the same fluid has found its place in the study of natural convection heat transfer and/or thermosolutal (double diffusive) convection. Such a composed cavity has wide ranges of industrial and environmental applications. Fibrous thermal insulation, solidification, fuel cell, cooling of nuclear fuel debris, solar collectors, and underground storage of radioactive waste are some of the many applications. According to its application, the confined layers may be vertically

Received 20 February 2013; accepted 10 September 2013.

Address correspondence to Ali Chamkha, Manufacturing Engineering Department, The Public Authority for Applied Education and Training, P.O. Box 42325, Shuweikh 70654, Kuwait. E-mail: achamkha@yahoo.com

NOMENCLATURE

A	aspect ratio, (H/L)	V	dimensionless velocity component along y-direction
Cp	specific heat at constant pressure, (J kg^{-1} K^{-1})	x,y	Cartesian coordinates, (m)
Da	Darcy number, $\mathrm{Da} = K/L^2$	X, Y	dimensionless Cartesian coordinates
g	gravitational field, (m s^{-2})	α	thermal diffusivity, (m^2 s^{-1})
H	cavity height, (m)	β	thermal expansion coefficient, (K^{-1})
k	thermal conductivity, (W m^{-1} K^{-1})	ε	porosity of the porous layer
K	permeability of porous medium, (m^2)	φ	nanoparticles volume fraction
kr	effective porous layer to nanofluid conductivities ratio, $kr = k_{eff}/k_{nf}$	μ	dynamic viscosity, (Pa · s)
		ν	kinematic viscosity, (m^{2}s^{-1})
L	cavity length, (m)	θ	dimensionless temperature
p	pressure, (Nm^{-2})	ρ	density, (kg m^{-3})
Pr	Prandtl number	ψ, Ψ	stream function (m^{2}s^{-1}), dimensionless stream function
Nu	average Nusselt number		
$\mathrm{Nu}_{l,r}$	local Nusselt, number along the left/right walls	ω, Ω	vorticity (s^{-1}), dimensionless vorticity
Ra	Rayleigh number $\mathrm{Ra} = g\beta_f(T_h - T_c)L^3/\nu_f\alpha_f$	**Subscripts**	
T	temperature, (K)	c	cold
u	velocity component along x-direction, (m s^{-1})	eff	effective
		f	fluid
v	velocity component along y-direction, (m s^{-1})	h	hot
		i	interface
U	dimensionless velocity component along x-direction	nf	nanofluid
		p	solid nanoparticles

separated or horizontally (i.e., fluid overlaying a porous layer). The interface between the two layers may be permeable or impermeable (no momentum exchange).

In an early study, Beavers and Joseph [1] have demonstrated, experimentally, that the no-slip condition due to the tangent velocity at the interface of a fluid flowing overlaying a porous layer is not verified. Theoretically, this was agreed when assuming the flow within the porous layer obeys the Darcy law. Limited published works regarding the impermeable interface were found as in Tong and Subramanian [2] and Sathe et al. [3]. Both studies have considered numerical analysis steady state natural convection in vertically divided rectangular enclosures. The Darcy model was adopted in reference [2] while the Darcy–Brinkman model was adopted in reference [3], who also considered the permeable interface. The main finding of these two studies was that for an impermeable interface, the heat transfer could be minimized by partially filling instead of entirely filling an enclosure with a porous medium. However, due to their essential applications, the partitioned cavity with a permeable interface has attracted vast attention in the literature. The horizontally partitioned cavity can be found in references [4–17]. A brief description of some of these works will be given here. Chen and Chen [4] have conducted experiments in a horizontal superposed fluid and porous layer contained in a test cavity. Three fluids were used while the porous layer consisted of 3 mm diameter glass beads. Their main experimental results were a steeper decrease in the critical Rayleigh number as the thickness of the fluid layer was increased and a sudden decrease in the critical waveform when the fluid layer thickness is between 0.1 and 0.2. In a numerical

investigation, the experimental results of reference [4] were verified by Kim and Choi [5]. Heat and mass transfer rates for natural convection driven by the temperature and concentration gradients in composite cavity was studied by Singh et al. [6]. They reported that the Darcy, thermal and solutal Rayleigh numbers played a great role on the fluid penetration into the porous layer. Also, the Nusselt number decreased while Sherwood number increased with an increase of the Lewis number. Hirata et al. [11] have performed a comparative study for the linear stability between the double–domain approach, using the classical Darcy model, and the one–domain approach. Their conclusion was that the Brinkman model term played a secondary role on the stability results. A locally heating, from below, was studied numerically basing on one–domain approach by Bagchi and Kulacki [15]. They recorded an adverse relation between the locally heating source size and the average Nusselt number. The average Nusselt number increased with the Darcy number. They also reported that the size of heat source did not affect the dependence of the Nusselt number on the porous layer thickness and Darcy number. The same co–workers, Bagchi and Kulacki [17], conducted an experimental study to ascertain their findings in reference [15]. Their cavity was simulated by a rectangular chamber with 3 mm diameter glass beads as the porous layer and distilled water as the saturating fluid. The effect of the porous layer thickness agreed with their conclusions in reference [15], but no clear effect of heater size was noticed.

Vertically divided porous-fluid or porous–fluid–porous cavities have received, somewhat, lesser attention especially in the experimental studies. Beckermann et al. [18] have, numerically and experimentally, performed a comprehensive analysis to study the natural convection with the fluid and porous layers. They found that the degree of penetration of fluid into the porous layer depended roughly on the product of the Rayliegh and Darcy numbers, which should be greater than about 50 in order for penetration to be significant. Natural convection in an enclosure composed of two porous layers, one adjacent to each vertical wall, with fluid layer occupied the central portion of the enclosure was studied by Oosthuizen and Paul [19]. The main conclusion that was drawn from their results was that a substantial increase in the heat transfer rate could be obtained by using layers of porous media and pure fluid. Beckermann and Viskanta [20] have reported a combined numerical and experimental study of solid/liquid phase change in porous media with natural convection in the melt region. They considered irregular interface of the constituents. They found that the interface shape was considerably influenced by the natural convection in the melt region as well as the heat conduction in the solid region. Goyean and Gobin [21] have focused their study on the influence of the porous layer permeability (Darcy number) and found the heat transfer results from a complex interaction between the viscous drag in the porous layer and the driven force enhancement due to the flow penetration. In contrast with reference [19], Mharzi et al. [22] have considered two fluid layers, one on each cavity side while the porous layer was included in the cavity center. In addition, they considered the thermosolutal convection. Extensive analytic study to natural convection flow in a partly porous cavity was reported by Mercier et al. [23]. Simple relationships were summarized to show the influence of the porous layer thickness, permeability, and the Rayleigh number on the flow structure and heat transfer. Bennacer et al. [24] have discussed the effect of anisotropicty of porous layers attached to the vertical walls and confining a fluid

at the cavity center on the thermosolutal and natural convection. They considered thermally and concentration driven flows. Little effect of the Darcy number on the rates of heat and mass transfer was recorded at high and low permeability regions. They recorded also a critical anisotropy parameter at which the Nusselt number was minimum. Due to their interest in such field of investigation, Gobin et al. [25] have focused on the analysis of the influence of the parameters governing double diffusive convection like the ratios of solutal and thermal parameters, the diffusivities and buoyancy forces.

Different geometries, but related to the subject of this paper can be found in references [26–28]. The two vertical layers of Merrikh and Mohamad [26] were both porous media. They studied the validity of the Darcy model. Their results showed that there is a difference in predictions between the Darcy and Brinkman models. A rectangular metal foam sample (of high porosity) localized on the bottom of a fluid–filled cavity and heated from below was studied numerically and experimentally by Phaikumar and Mahaja [27]. In other words, they had two, vertical and horizontal interfaces. The double diffusive natural convection between a fluid and overlaying a porous medium with stepped interface was investigated by Baytas et al. [28]. Dramatic changes of the heat and mass transfer were recorded in this case.

However, to the authors' best knowledge, all of the considered fluids in this field of study were pure fluids like water, air, glycerin, etc. Nanofluids, which have attracted a significant attention about one decade ago (Choi [29], Tiwari and Das [30], Ghasemi and Aminossadati [31]) have not found their place in the fluid–porous layers partitioned cavities at all. Therefore, the authors believe that it is a valuable idea to initiate a study of natural convection in a vertical cavity consisting of two layers, a nanofluid layer and porous medium layer saturated by the same nanofluid. The interface separating them is assumed to be permeable. It is sought that this study will reveal the contributions of nanofluids in the performance of the partially filled–porous cavities, which has an industrial application importance.

2. MATHEMATICAL MODELING

The considered problem is shown schematically in Figure 1. It is a rectangular cavity of width L and height H. A vertical porous layer of thickness xp is localized on the left part of cavity and saturated with a nanofluid. This nanofluid fills the remainder of the cavity (L-xp). The left vertical wall of the cavity which is in contact with the porous layer is heated isothermally and kept at T_h, while the right wall of the cavity is cooled isothermally and kept at T_c. All outer boundaries are assumed to be impermeable, while the vertical interface between the nanofluid and porous layers is assumed permeable. Regarding the porous layer, uniform and undeformable pores are assumed. The nanofluid is composed of a base fluid (water) and solid Copper nanoparticles. They (the base fluid and the nanoparticles) are assumed to be in thermal equilibrium and no slip occurs between them. In addition, a thermal equilibrium between the nanofluid filling pores and the solid matrix is assumed. The natural convection flow is assumed steady, laminar, and with constant physical properties except the density where it varies with temperature according to Boussinesq approximation. Moreover, the Soret and Dufour effect are neglected.

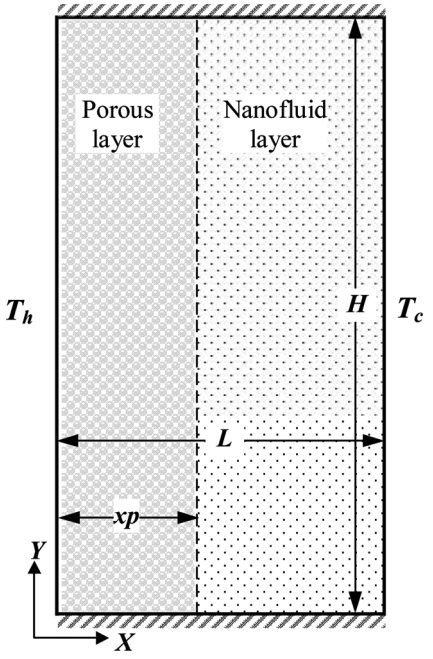

Figure 1. Physical domain.

Mathematically, there exist two approaches for dealing with porous–fluid layer cavity, namely, the single–domain and the double–domain approaches. The former puts one set of governing equations for both layers with a binary parameter that modifies the momentum equation to be applicable in any layer. It is simple and requires less boundary conditions. But it is restricted by formulating the grid in such a manner that no grids located along the fluid–porous interface. On the other hand, the double–domain approach employs a separated set of equations for each layer. The two sets are matched by appropriate boundary conditions along the interface. In the present study, and to avoid the restriction of the grid localization due to the interface, the double–domain approach is used. The Darcy–Brinkman model is invoked to represent the convection within the porous layer, where in this model, there is no problem in the order of the matched momentum equation in the nanofluid and porous layers. The dimensional governing equations for the porous layer are as follows.

Continuity:

$$\frac{\partial u_p}{\partial x} + \frac{\partial v_p}{\partial y} = 0 \tag{1}$$

x–direction momentum equation:

$$\rho_{nf}\left(u_p\frac{\partial u_p}{\partial x} + v_p\frac{\partial u_p}{\partial y}\right) = -\varepsilon^2\frac{\partial p}{\partial x} + \varepsilon\mu_{nf}\left(\frac{\partial^2 u_p}{\partial x^2} + \frac{\partial^2 u_p}{\partial y^2}\right) - \varepsilon^2\frac{\mu_{nf}}{K}u_p \tag{2}$$

y–direction momentum equation:

$$\rho_{nf}\left(u_p\frac{\partial v_p}{\partial x}+v_p\frac{\partial v_p}{\partial y}\right)=-\varepsilon^2\frac{\partial p}{\partial y}+\varepsilon\mu_{nf}\left(\frac{\partial^2 v_p}{\partial x^2}+\frac{\partial^2 v_p}{\partial y^2}\right)-\varepsilon^2\frac{\mu_{nf}}{K}v_p$$
$$+\varepsilon^2\beta_{nf}\rho_{nf}g\left(T_p-T_o\right) \tag{3}$$

Energy equation:

$$u_p\frac{\partial T_p}{\partial x}+v_p\frac{\partial T_p}{\partial y}=\alpha_{eff}\left(\frac{\partial^2 T_p}{\partial x^2}+\frac{\partial^2 T_p}{\partial y^2}\right) \tag{4}$$

The dimensional equations of the nanofluid layer are as follows. Continuity:

$$\frac{\partial u_{nf}}{\partial x}+\frac{\partial v_{nf}}{\partial y}=0 \tag{5}$$

x–direction momentum equation:

$$\rho_{nf}\left(u_{nf}\frac{\partial u_{nf}}{\partial x}+v_{nf}\frac{\partial u_{nf}}{\partial y}\right)=-\frac{\partial p}{\partial x}+\mu_{nf}\left(\frac{\partial^2 u_{nf}}{\partial x^2}+\frac{\partial^2 u_{nf}}{\partial y^2}\right) \tag{6}$$

y–direction momentum equation:

$$\rho_{nf}\left(u_{nf}\frac{\partial v_{nf}}{\partial x}+v_{nf}\frac{\partial v_{nf}}{\partial y}\right)=-\frac{\partial p}{\partial y}+\mu_{nf}\left(\frac{\partial^2 v_{nf}}{\partial x^2}+\frac{\partial^2 v_{nf}}{\partial y^2}\right)+\beta_{nf}\rho_{nf}g\left(T_{nf}-T_o\right) \tag{7}$$

Energy equation:

$$u_{nf}\frac{\partial T_{nf}}{\partial x}+v_{nf}\frac{\partial T_{nf}}{\partial y}=\alpha_{nf}\left(\frac{\partial^2 T_{nf}}{\partial x^2}+\frac{\partial^2 T_{nf}}{\partial y^2}\right) \tag{8}$$

Where ε is the porosity of the porous medium, β is the thermal expansion coefficient, ρ is the density, K is the permeability of the porous medium, μ is the dynamic viscosity, and α is the thermal diffusivity. The subscripts p and nf stand for solid nanoparticles and nanofluid, respectively. The pressure gradient term is eliminated from each set of momentum equations by following the usual procedure. Basing the formulation according to stream function $u=\frac{\partial\psi}{\partial y}$, $v=-\frac{\partial\psi}{\partial x}$ and vorticity $\omega=\frac{\partial v}{\partial x}-\frac{\partial u}{\partial y}$ and introducing the following nondimensional parameters, $X=\frac{x}{L}$, $Y=\frac{y}{L}$, $Xp=\frac{xp}{L}$, $\Psi=\frac{\psi}{\alpha_f}$, $\Omega=\frac{\omega L^2}{\alpha_f}$, $\theta=\frac{T-T_c}{T_h-T_c}$, Rayleigh number $\mathrm{Ra}=\frac{g\beta_f(T_h-T_c)L^3}{\nu_f\alpha_f}$, Prandtl number $\mathrm{Pr}=\frac{\nu_f}{\alpha_f}$, and Darcy number $\mathrm{Da}=\frac{K}{L^2}$, together with the adopted relations that prescribe the physical properties of the nanofluid which are considered to be depended on the nanoparticles volume fraction φ only and as follows.

$$\rho_{nf}=(1-\varphi)\rho_f+\varphi\rho_p \tag{9}$$

$$(\rho\beta)_{nf}=(1-\varphi)(\rho\beta)_f+\varphi(\rho\beta)_p \tag{10}$$

Thermal diffusivity (Abu-Nada and Oztop [32]):

$$\alpha_{nf} = \frac{k_{nf}}{(\rho Cp)_{nf}} \tag{11}$$

$$\alpha_{eff} = \frac{k_{eff}}{(\rho Cp)_{nf}} \tag{12}$$

$$k_{eff} = (1-\varepsilon)k_s + \varepsilon k_{nf} \tag{13}$$

Heat capacity (Khanafer et al. [33]):

$$(\rho Cp)_{nf} = (1-\varphi)(\rho Cp)_f + \varphi(\rho Cp)_p \tag{14}$$

Thermal conductivity, based on Maxwell-Garnetts:

$$k_{nf} = \frac{(k_p + 2k_f) - 2\varphi(k_f - k_p)}{(k_p + 2k_f) + \varphi(k_f - k_p)} k_f \tag{15}$$

Viscosity (Brinkman [34]):

$$\mu_{nf} = \frac{\mu_f}{(1-\varphi)^{2.5}} \tag{16}$$

Where k and (ρCp) represent the thermal conductivity and heat capacity, respectively. Maxwell-Garanetts and Brinkman models are widely used in describing the nanofluid conductivity and viscosity, respectively as they proven to give reasonable results in many different studies [35–38]. Nevertheless, more sophisticated models are also investigated [39]. However, the nondimensional set of conservation equations can be written as follows for the porous layer.

Continuity:

$$\frac{\partial^2 \Psi_p}{\partial X^2} + \frac{\partial^2 \Psi_p}{\partial Y^2} = -\Omega_p \tag{17}$$

Momentum:

$$\begin{aligned} &\frac{\partial \Psi_p}{\partial Y}\frac{\partial \Omega_p}{\partial X} - \frac{\partial \Psi_p}{\partial X}\frac{\partial \Omega_p}{\partial Y} = \frac{\rho_f}{\rho_{nf}(1-\varphi)^{2.5}}\varepsilon \,\mathrm{Pr}\left(\frac{\partial^2 \Omega_p}{\partial X^2} + \frac{\partial^2 \Omega_p}{\partial Y^2}\right) \\ &- \frac{\rho_f}{\rho_{nf}(1-\varphi)^{2.5}}\frac{\varepsilon^2 \,\mathrm{Pr}}{\mathrm{Da}}\Omega_p + \frac{(\rho\beta)_{nf}}{\rho_{nf}\beta_f}\varepsilon^2 \mathrm{Ra}\ \mathrm{Pr}\frac{\partial \theta_p}{\partial X} \end{aligned} \tag{18}$$

Energy:

$$\frac{\partial \Psi_p}{\partial Y}\frac{\partial \theta_p}{\partial X} - \frac{\partial \Psi_p}{\partial X}\frac{\partial \theta_p}{\partial Y} = \frac{\alpha_{eff}}{\alpha_f}\left(\frac{\partial^2 \theta_p}{\partial X^2} + \frac{\partial^2 \theta_p}{\partial Y^2}\right) \tag{19}$$

Nanofluid: Continuity:

$$\frac{\partial^2 \Psi_{nf}}{\partial X^2} + \frac{\partial^2 \Psi_{nf}}{\partial Y^2} = -\Omega_{nf} \tag{20}$$

Momentum:

$$\frac{\partial \Psi_{nf}}{\partial Y}\frac{\partial \Omega_{nf}}{\partial X} - \frac{\partial \Psi_{nf}}{\partial X}\frac{\partial \Omega_{nf}}{\partial Y} = \frac{\rho_f}{\rho_{nf}(1-\varphi)^{2.5}}$$
$$\Pr\left(\frac{\partial^2 \Omega_{nf}}{\partial X^2} + \frac{\partial^2 \Omega_{nf}}{\partial Y^2}\right) + \frac{(\rho\beta)_{nf}}{\rho_{nf}\beta_f}\mathrm{Ra}\ \Pr\frac{\partial \theta_{nf}}{\partial X} \tag{21}$$

Energy:

$$\frac{\partial \Psi_{nf}}{\partial Y}\frac{\partial \theta_{nf}}{\partial X} - \frac{\partial \Psi_{nf}}{\partial X}\frac{\partial \theta_{nf}}{\partial Y} = \frac{\alpha_{nf}}{\alpha_f}\left(\frac{\partial^2 \theta_{nf}}{\partial X^2} + \frac{\partial^2 \theta_{nf}}{\partial Y^2}\right) \tag{22}$$

The conditions on the outer boundaries of the cavity are as follows.

$$\Psi = 0, \theta = 1, \Omega = -(\partial^2 \Psi/\partial Y^2) \text{ at } X = 0$$
$$\Psi = 0, \theta = 0, \Omega = -(\partial^2 \Psi/\partial Y^2) \text{ at } X = 1$$
$$\Psi = 0, \partial\theta/\partial Y = 0, \Omega = -(\partial^2 \Psi/\partial X^2) \text{ at } Y = 0, A$$

The interface boundary conditions are derived from equating (continuity) of tangential and normal velocities, shear and normal stresses, temperature, and the heat flux across the interface, and assuming the same dynamic viscosity ($\mu_p = \mu_{nf}$) in both layers. Hence, the interface conditions can be written as follows

$$\theta_p = \theta_{nf} \quad \frac{\partial \theta_{nf}}{\partial X} = \frac{k_{eff}}{k_{nf}}\frac{\partial \theta_p}{\partial X} \tag{23a}$$

$$\Psi_p = \Psi_{nf} \quad \frac{\partial \Psi_{nf}}{\partial X} = \frac{\partial \Psi_p}{\partial X} \tag{23b}$$

$$\Omega_p = \Omega_{nf} \quad \frac{\partial \Omega_{nf}}{\partial X} = \frac{\partial \Omega_p}{\partial X} \tag{23c}$$

3. NUMERICAL SOLUTION

The rectangular domain was descretized into m horizontal grids and n vertical grids. The governing equations (17–22) were solved numerically using the central finite difference method, Gauss-Seidel iteration procedure with successive under relaxation (SUR) method is followed in the solution. The convective terms of the momentum and energy equations were treated by the upwind scheme to attain the solution stability. The stream function, vorticity, and dimensionless temperature

are to be calculated from continuity, momentum, and energy equations, respectively. Along the outer boundaries, the condition on Ω was interpreted using Wilkes formula [39] as follows.

$$\Omega_{o,j} = -\frac{8\Psi_{o+1,j} - \Psi_{o+2,j}}{2\Delta n^2} \tag{24}$$

where o represents the boundary node and Δn is the interval normal to this boundary.

The conditions on the impermeable interface (Eqs. (23*a*) and (23*b*)) are interpreted numerically by taking three points backward gradient for the porous layer and three points forward gradient through the nanofluid layer. Accordingly, the following difference equations are invoked to compute the interface potentials:

$$\Psi_i(i,j) = \frac{4\Psi_{nf}(i+1,j) - \Psi_{nf}(i+2,j) + 4\Psi_p(i-1,j) - \Psi_p(i-2,j)}{6} \tag{25a}$$

$$\Omega_i(i,j) = \frac{4\Omega_{nf}(i+1,j) - \Omega_{nf}(i+2,j) + 4\Omega_p(i-1,j) - \Omega_p(i-2,j)}{6} \tag{25b}$$

$$\theta_i(i,j) = \frac{4\theta_{nf}(i+1,j) - \theta_{nf}(i+2,j) + kr\big(4\theta_p(i-1,j) - \theta_p(i-2,j)\big)}{3(1+kr)} \tag{25c}$$

Where, $kr = k_{eff}/k_{nf}$ is the ratio of the effective thermal conductivity of the porous layer (Eq. (13)) to the thermal conductivity of the nanofluid (Eq. (15)).

The iteration is terminated when the following criterion is satisfied:

$$\max\left|\left[\frac{\chi_{new}(i,j) - \chi_{old}(i,j)}{\chi_{old}(i,j)}\right]\right| \le 10^{-6} \tag{26}$$

where χ denotes any variable, Ψ, Ω, or θ. It is found the grid size that gives stable solution and faster convergence is highly sensitive to Rayleigh number and the aspect ratio, and less for the other parameters. This was concluded by conducting an extensive mesh testing procedure to guarantee a grid independent solution. Various mesh combinations were explored for $A = 1$, 2, 4, and $\mathrm{Ra} = 10^6$, $\mathrm{Da} = 10^{-6}$, $Xp = 0.2$, $\mathrm{Pr} = 6.26$, and $\varphi = 0.01$. The present code was tested for grid independency by calculating the average Nusselt numbers on the left and right walls and the maximum stream function in addition. Accordingly, and as a compromise among the solution stability and the speed of convergence and the computational time, the following grids were invoked; 61×61 for $A = 1$, 61×81 for $A = 2$, and 61×201 for $A = 4$. Another grid sizes were tested for different parameters, the results have confirmed the adequacy of the selected above three grid sizes.

Along the left wall, the local and average Nusselt numbers are calculated, respectively, from the following formulas:

$$\mathrm{Nu}_l = \frac{k_{eff}}{k_f}\left(\frac{\partial\theta_p}{\partial X}\right)_{X=0} \tag{27}$$

$$\mathrm{Nu} = \frac{1}{A}\frac{k_{eff}}{k_f}\int_0^A \left(\frac{\partial \theta_p}{\partial X}\right)_{X=0} dY \tag{28}$$

On the other hand, along the right wall, the local and average Nusselt numbers are calculated, respectively, from the following formulas:

$$\mathrm{Nu}_r = \frac{k_{nf}}{k_f}\left(\frac{\partial \theta_{nf}}{\partial X}\right)_{X=1} \tag{29}$$

$$\mathrm{Nu} = \frac{1}{A}\frac{k_{nf}}{k_f}\int_0^A \left(\frac{\partial \theta_{nf}}{\partial X}\right)_{X=1} dY \tag{30}$$

During the grid dependency test, the conformity between the average Nusselt numbers along the left and right walls was within 99%.

To ascertain the confidence of the present formulation, the present code was checked against three different cases, these; cavities fully–filled by pure fluid (De Vahl Davis [41]), nanofluid (Khanafer et al. [33]), and fully porous cavity (Lauriat and Prasad [42]), all of them are differentially heated. The parameters and the average Nusselt numbers of these three cases are presented in details in Table 1. Good agreement between the present code and what they reported despite the various numerical methods they used. Moreover, the validity is checked further by examining the horizontal U and vertical V components at mid planes $X = 0.5$, $Y = A/2$, respectively, with what is reported by Das and Sahoo [43]. This case is a differentially heated fully–filled porous cavity with internal heat generation. The results are illustrated in Figure 2 and very good agreement is obtained with V component, meanwhile a discrepancy exists with U component. This may be attributed to the difference in formulation followed by reference [43]. However, the results of the present code which is written in FORTRAN could be relied on.

Table 1. Comparisons of present numerical solutions with previous works of different cases

Case 1	Ra		de Vahl Davis [41]	Present
Pure fluid–filled cavity, Pr = 0.71	10^3		1.118	1.13
	10^5		4.519	4.55
	10^6		8.799	8.9
Case 2	Gr (RaPr)	φ	Khanafer et al. [33]	Present
Nanofluid–filled cavity, Pr = 6.2	10^3	0.04	2.08	2.029
	10^3	0.08	2.24	2.17
	10^5	0.04	8.93	8.55
	10^5	0.08	9.6	9.25
Case 3	Ra	Da	Lauriat and Prasad [42]	Present
Porous cavity, Pr = 1.0, ε = 0.4	10^3	10^{-2}	1.02	1.022
	10^5	10^{-2}	3.8	3.5
	10^7	10^{-6}	1.08	1.042
	10^8	10^{-6}	2.99	2.98

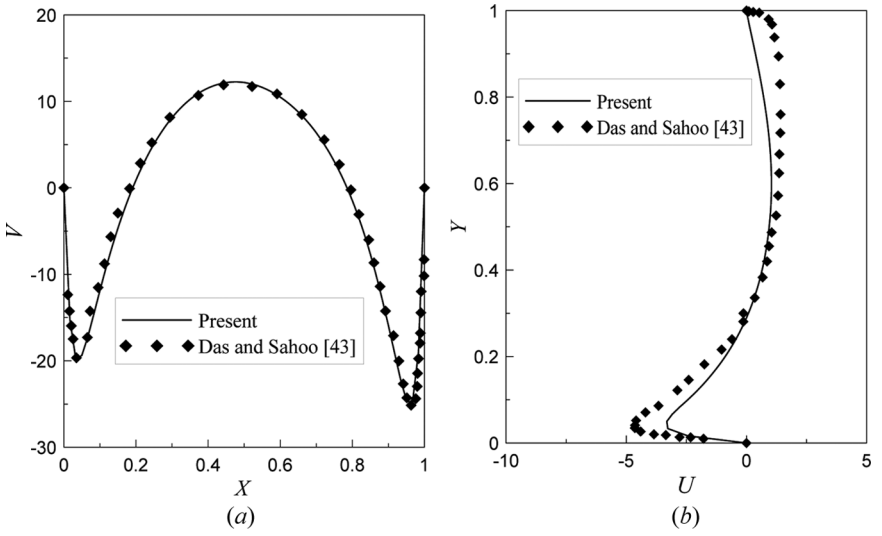

Figure 2. (*a*) Vertical and (*b*) horizontal velocities distribution along mid planes for porous cavity $Ra = 10^5$, $Da = 10^{-4}$, $A = 1$, $Pr = 1$, and $\varepsilon = 0.4$ with internal heat generation ($Q = 100$) (comparison with [42]).

4. RESULTS AND DISCUSSION

This section presents the numerical results in graphical form to illustrate the influence of the studied parameters on the flow and heat transfer characteristics. The nanofluid is considered to be composed of water base fluid ($Pr = 6.26$) and Cu nanoparticles (with physical properties shown in Table 2 [44, 45]). The porosity of the porous layer is fixed at $\varepsilon = 0.398$, which corresponds to 3 mm diameter glass beads of thermal conductivity $k_s = 0.845\,W/m \cdot K$. The ranges of the studied parameters are as follows: $Ra = 10^3$–10^6, $Da = 10^{-7}$–1, $Xp = 0$–0.9, $\varphi = 0$–0.1, and $A = 1$, 2, and 4.

Figure 3 presents contour maps of the streamlines and isotherms for $Ra = 10^5$, $Da = 10^{-5}$, $A = 2$, and for different porous layer thicknesses Xp. A single–cellular, clockwise rotating (negative streamline) cell is seen. For all Xp values, Figure 3*a*–3*c*, the nanofluid cell ($\varphi = 0.05$) is stronger than for a pure fluid ($\varphi = 0$). This refers to that increasing φ leads to an increase in the thermal conductivity (Eq. (15)), viscosity (Eq. (16)) and density (Eq. (9)) of the nanofluid. It can be inferred, hence, that the nanofluid receives enough thermal energy which leads to accelerate the flow and overcome the retardation effect of the viscous and inertia forces. The effect of the

Table 2. Thermophysical properties of base fluid and nanoparticles [44, 45]

Physical property	Base fluid (water)	Cu
Cp (J/kg/K)	4179	385
ρ (kg/m^3)	997.1	8933
k (W/m/K)	0.613	401
$\beta \times 10^{-5}$ (1/K)	21	1.67

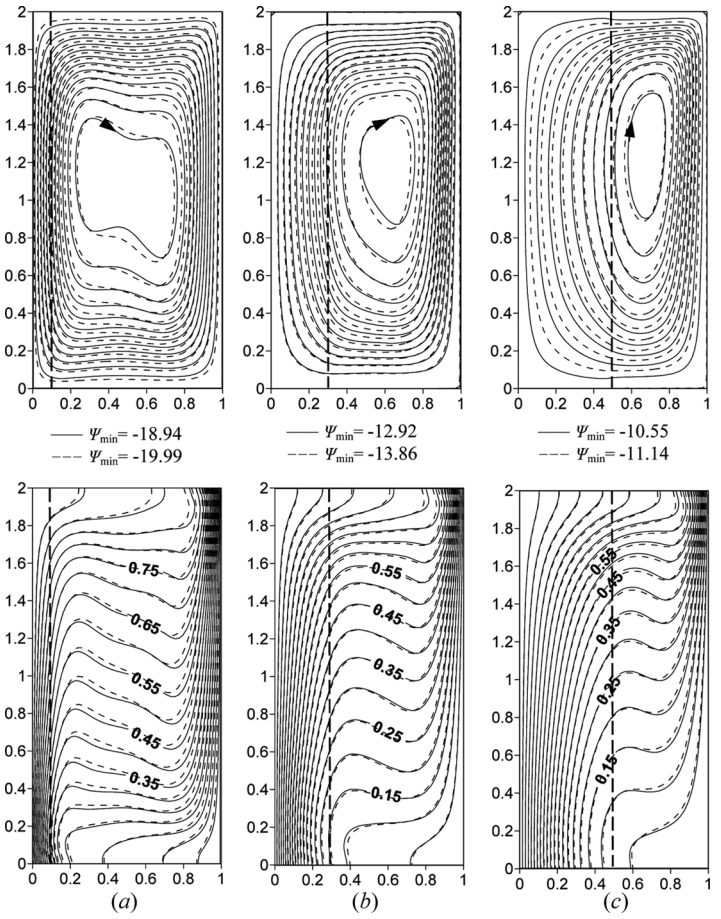

Figure 3. Streamlines (upper row) and isotherms (lower row) for $\mathrm{Ra} = 10^5$, $\mathrm{Da} = 10^{-5}$, $A = 2$, $\varphi = 0$ (solid lines), and $\varphi = 0.05$ (dashed lines). (*a*) $Xp = 0.1$, (*b*) $Xp = 0.3$, and (*c*) $Xp = 0.5$.

porous layer thickness Xp can be sensed by the reduction in the strength of the cell with increasing values of Xp. This is because of the hydrodynamic resistances offered by the porous layer. Within the porous layer, the penetrated streamlines show higher gradient at a lower thickness. However, at lower value of Xp (Figure 3*a*), a contracted central cell is seen and when Xp is increased, Figures. 3*b* and 3*c*, the cell tends to be vertically elongated. The isotherms (the lower row of Figure 3) appear to be less influenced by the 5% volume fraction of nanoparticles. The mostly vertical isotherms pattern within the porous layers indicates the dominance of the conduction heat transfer while the mostly horizontally isotherms pattern within the nanofluid layer implies the dominance of the convection mode heat transfer. Therefore, it is expected that the Nusselt number decreases with increasing values of Xp.

The effect of the nondimensional permeability (Darcy number) of 0.3 porous layer thickness is shown in Figure 4 for $\mathrm{Ra} = 10^5$ and $A = 2$. It can be seen from this

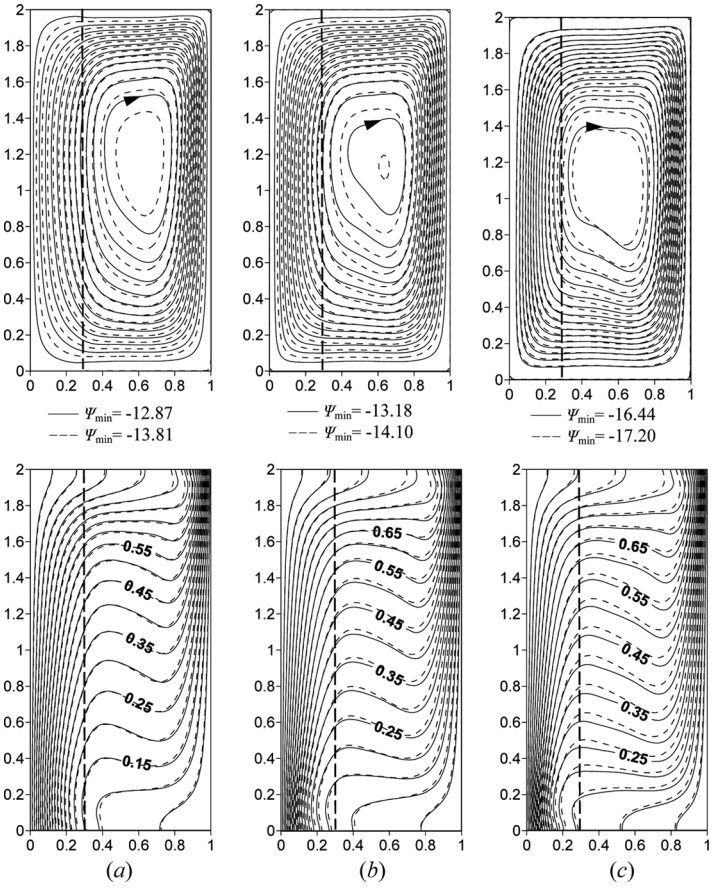

Figure 4. Streamlines (upper row) and isotherms (lower row) for $\mathrm{Ra} = 10^5$, $A = 2$, $Xp = 0.3$, $\varphi = 0$ (solid lines), and $\varphi = 0.05$ (dashed lines). (*a*) $\mathrm{Da} = 10^{-7}$, (*b*) $\mathrm{Da} = 10^{-4}$, and (*c*) $\mathrm{Da} = 10^{-1}$.

figure that increasing Da means increasing the porous layer permeability and therefore, more nanofluid is allowed to penetrate the porous layer and as a result, the strength of the cell is significantly increased. The remarkable object that can be drawn from Figure 4 is that the streamlines within the low permeability porous layer (Figure 4*a*) are more affected by the nanoparticles addition than the high permeability one (Figure 4*c*). This can be easily seen from the $|\Psi|_{max}$ values labeled on Figure 4, where for $\mathrm{Da} = 10^{-7}$, 10^{-4}, 10^{-1}, the percentage increase in $|\Psi|_{max}$ that is gained from adding 5% of Copper nanoparticles to pure water are 7.3%, 7% and 4.6%, respectively. The isotherms of Figure 4 show how the convection is transmitted from the nanofluid layer to the porous layer with increasing in the permeability of the porous layer.

Figure 5 depicts the variations of the streamlines and isotherms contour maps with the Rayleigh number for $\mathrm{Da} = 10^{-5}$, $Xp = 0.3$, and $A = 2$. The streamlines contours intervals of $\mathrm{Ra} = 10^3$, 10^4, and 10^6 are 0.25, 0.5 and 1, respectively, and this is done to avoid the ill–conditioning of the crowded streamlines of higher Ra values.

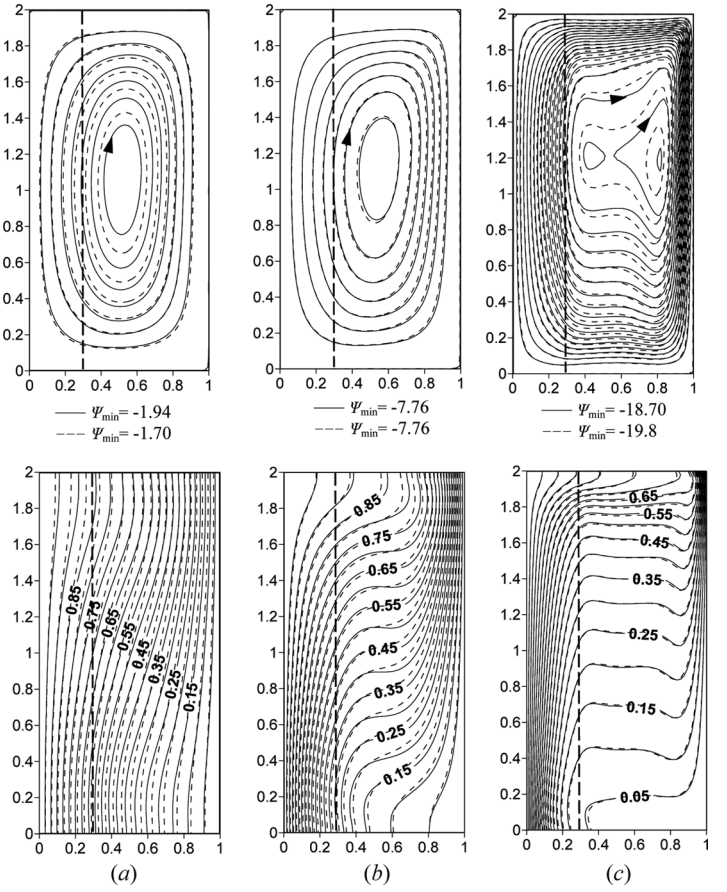

Figure 5. Streamlines (upper row) and isotherms (lower row) for $\mathrm{Da} = 10^{-5}$, $Xp = 0.3$, $A = 2$, $\varphi = 0$ (solid lines), and $\varphi = 0.05$ (dashed lines). (*a*) $\mathrm{Ra} = 10^3$, (*b*) $\mathrm{Ra} = 10^4$, and (*c*) $\mathrm{Ra} = 10^6$.

Nevertheless, the streamlines appear denser at high values of Ra due to the strong circulation. At $\mathrm{Ra} = 10^3$ Figure. 5*a*, the circulating map gives an appearance of no effect to the porous layer. Moreover, the strength of the circulation is reduced by adding nanoparticles. This reduction comes from the retardation effect occurring in the porous layer at a specified Ra value. This phenomenon was extensively discussed in our previous work [45]. At a higher Ra value (Figure 5*c*), the central cell is extended noticeably within the nanofluid layer and therefore, a significant penetration of streamlines towards the porous layer is occurred. However, at an intermediate Ra value (Figure 5*b*), there is no effect of the nanoparticles on the overall streamlines which means equivalent effects of the thermal energy increase, the drag and viscous forces. The isotherms corresponding to these cases (the lower row of Figure 5*a*) reflect primarily that the convection is gained with Ra and especially within the nanofluid layer.

Figure 6 presents the effect of the aspect ratio ($A = 1$, 4) for $\mathrm{Ra} = 10^5$, $\mathrm{Da} = 10^{-5}$, and $Xp = 0.3$. The middle column of Figure 3 ($A = 2$) can be called

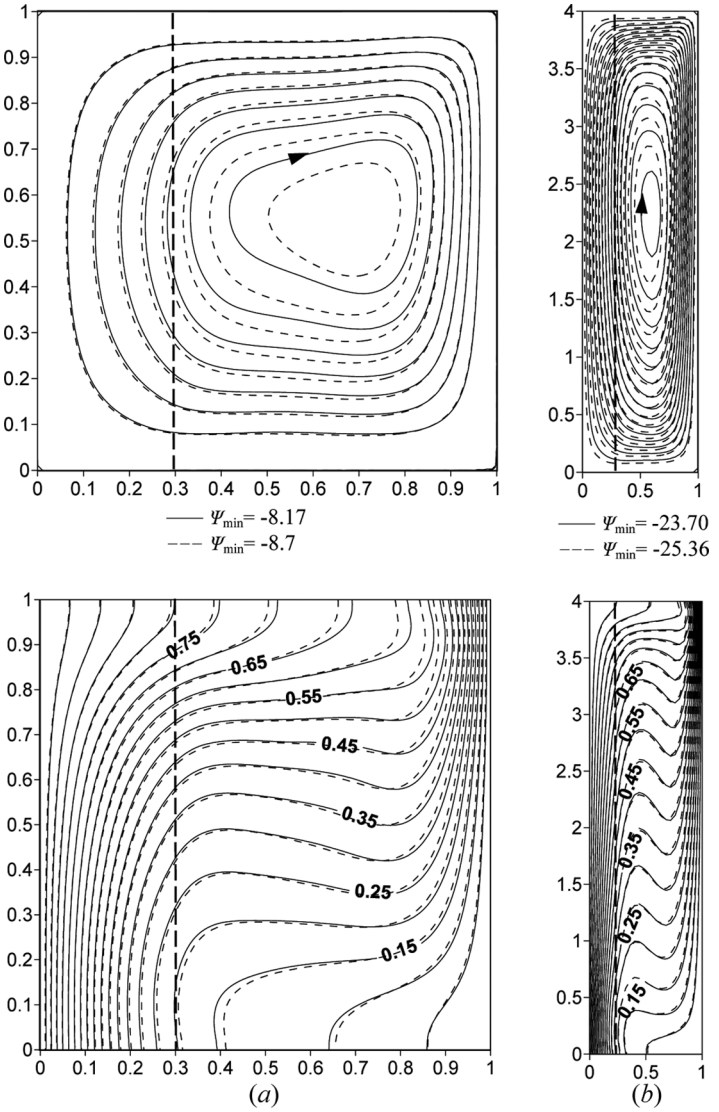

Figure 6. Streamlines (upper row) and isotherms (lower row) for $\mathrm{Ra} = 10^5$, $\mathrm{Da} = 10^{-5}$, $Xp = 0.3$, $\varphi = 0$ (solid lines), and $\varphi = 0.05$ (dashed lines). (*a*) $A = 1$, and (*b*) $A = 4$.

here for comparison purpose. When $A = 1$, the central cell plumed towards the interface between the nanofluid and porous layers. Increasing A to 2 and 4 causes the streamlines structure to keep its single cellular mode with vertically elongated central cell towards the top and bottom of the cavity. Because of no flow across these two sides, a large penetration of flow is seen within the porous layer. This is clear in Figure 6*b* where a dense appearance of streamlines occurs despite the fact that the line interval is twice than those of $A = 1$ and 2. From the maximum value of $|\Psi|$ labeled on Figure 6 and Figure 3b, an aspect ratio of $A = 2$ offers the greatest

strength enhancement which is 7.3% due to the nanofluid effect. There is no significant feature recorded by varying the aspect ratio on the isotherms.

The distribution of the vertical velocity component V and the dimensionless temperature θ are examined along the X–axis at $Y = A/2$ for $\mathrm{Ra} = 10^6$ and for various ranges of the other parameters. The results are presented in Figure 7. Figure 7*a* shows that within the porous layer, the flow is slightly accelerated with pure conduction heat transfer when φ is increased. On the other hand, increasing of φ increases both the thermal and hydrodynamic layers adjacent to the right cold

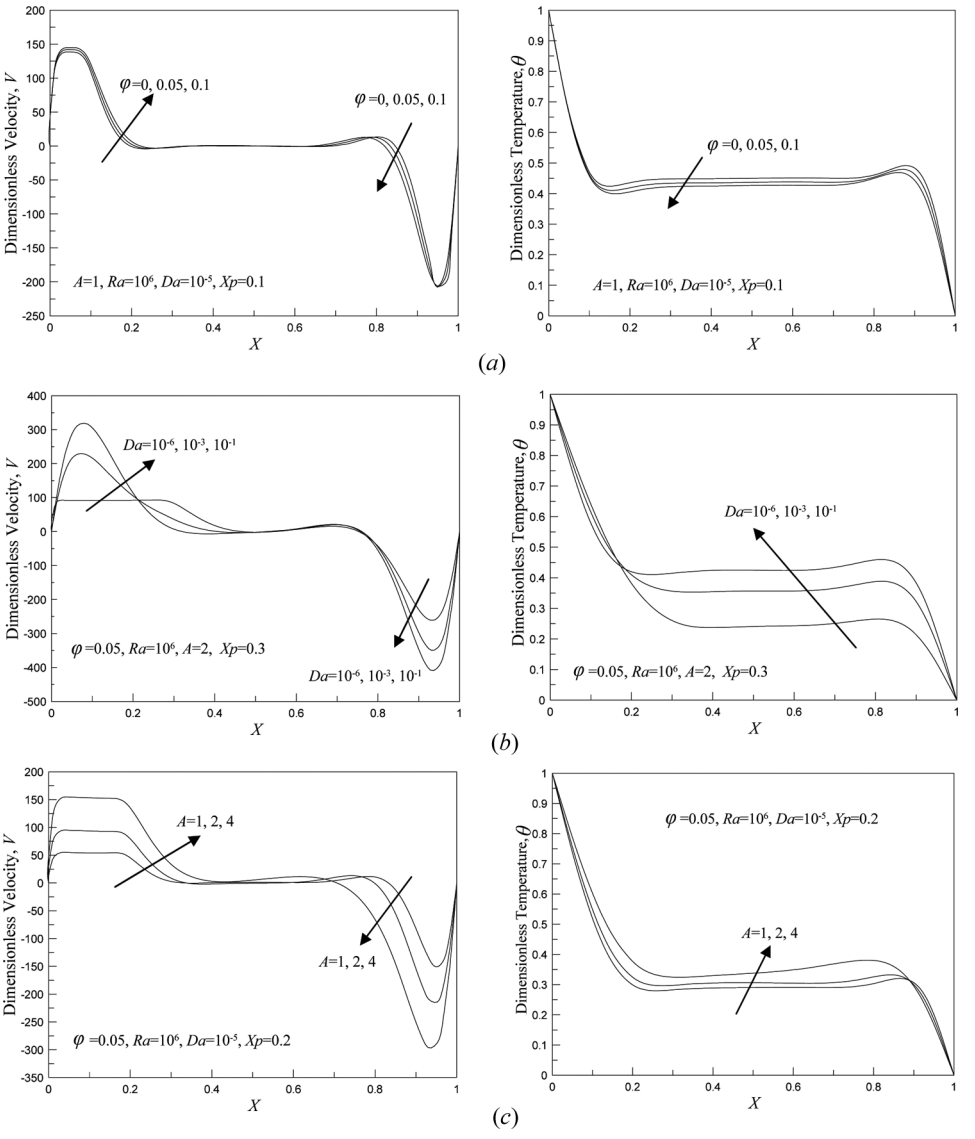

Figure 7. Local distribution of vertical velocity component (right) and dimensionless temperature (left) along X–axis at $Y = A/2$, (*a*) φ effect, (*b*) Da effect, and (*c*) A effect.

wall. Figure 7*b* depicts the effect of the Darcy number Da. The velocity profile within the porous layer is transmitted from flattened to parabolic with increasing Da, i.e., increasing the permeability of the porous medium which means less hydrodynamic resistance. This in turn, affects also the flow structure adjacent to the right cold wall and the temperature distribution within the fluid layer. Convection heat transfer within the porous layer is seen to be onset at high Da values. Figure 7*c* presents the effect of the aspect ratio. It is clear from this figure how the extra vertical space available leads to acceleration and expansion of the fluid hydrodynamic boundary layer. The conduction mode is, mostly, dominated within the porous layer. However, it is worth mentioning that the positive peaks of the vertical velocity within the porous layer are smaller than those of the negative peaks adjacent to the right wall

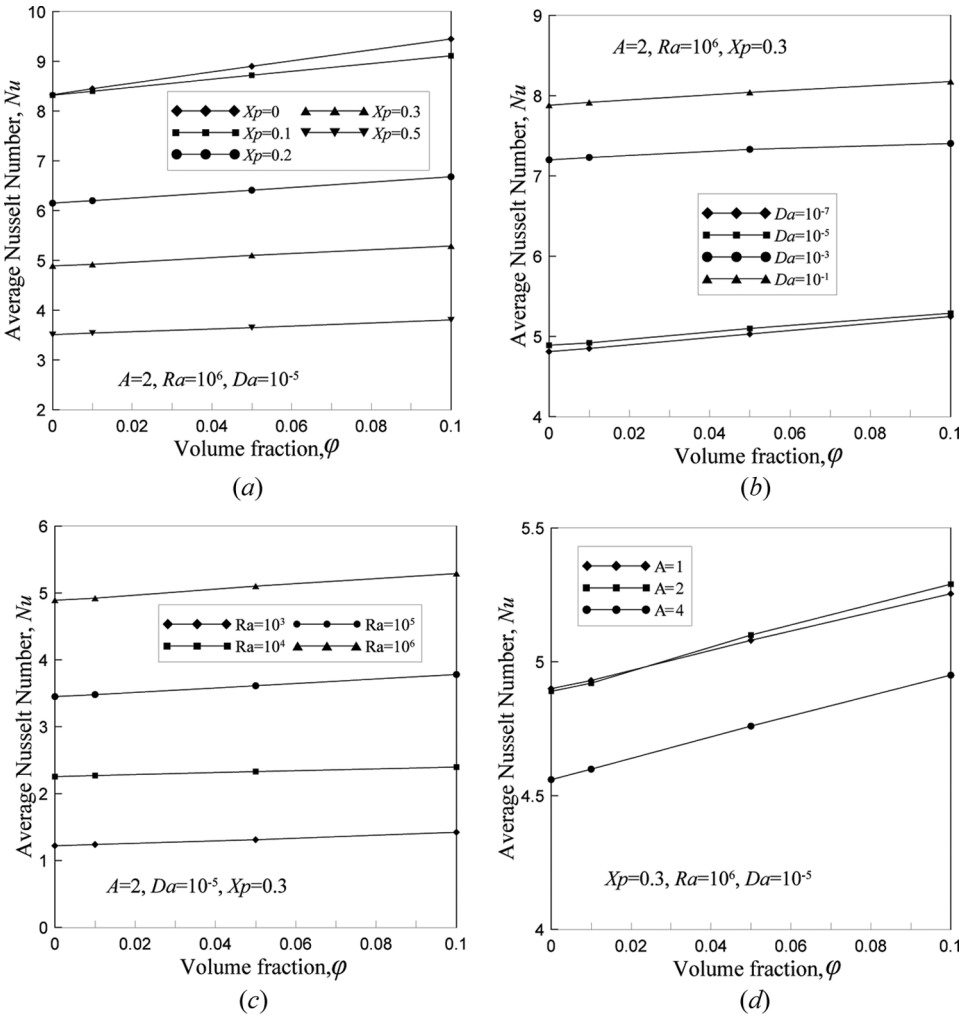

Figure 8. Variations of Nusselt number Nu with nanoparticles volume fractions, (*a*) *Xp* effect, (*b*) Da effect, (*c*) Ra effect, and (*d*) *A* effect.

of the nanofluid layer. This is axiomatic, due to the hydrodynamic resistances difference between the two layers.

To get a more understanding about the effects of the studied parameters, the overall heat transfer represented by the average Nusselt number over the heated wall is investigated extensively through the following figures.

Figure 8 presents the positive feature of using a nanofluid in composite cavities. That is, the heat transfer is enhanced with increasing values of φ regardless of the values of the other parameters and despite the existence of the porous layer which resists the heat transfer as it is clearly evident in Figure 8*a*, where the slope of $Xp = 0$ curve is greater than the other Xp values curves. Figure 8*b* tells us that the permeability of the porous layer does not affect the enhancement action of the nanoparticles. For all Ra values, the deterioration of Nu is not seen as demonstrated in Figure 8*c*. In addition, the aspect ratio variation does not alter the positive action of the nanofluid enhancement as shown in Figure 8*d*. But between leaving this figure, it is worth pointing out that the aspect ratio $A = 2$, offers a maximum value of Nu for $Xp = 0.3$ and when $\varphi > 0.02$.

It is well known that by increasing the porous layer thickness, a corresponding reduction in Nu is obtained. But we found in this study, in some situations and precisely at a lower value of Ra, increasing Xp to 0.1 leads to an increase in Nu, then, further increase of Xp leads to a steep decrease in the value of Nu, as shown in Figure 9*a*. This behavior is attributed to the fact that the effective thermal conductivity of the porous layer (Eq. (13)) is larger than that of the nanofluid layer (Eq. (15)) and therefore, the gained thermal energy due to conductivity when $Xp = 0.1$ overcomes the hydrodynamic resistance produced by the porous layer. When Xp is larger than 0.1, the influence of the effective thermal conductivity and the hydrodynamic resistance are inversed. This feature disappears when $\mathrm{Ra} = 10^6$ (Figure 9*b*), i.e., Nu decreases with all Xp values. This is because of the fact that at $\mathrm{Ra} = 10^6$, the penetrated flow into the porous layer is not influenced by the acceleration raised from the thermal energy experienced by the higher effective thermal conductivity of the porous layer.

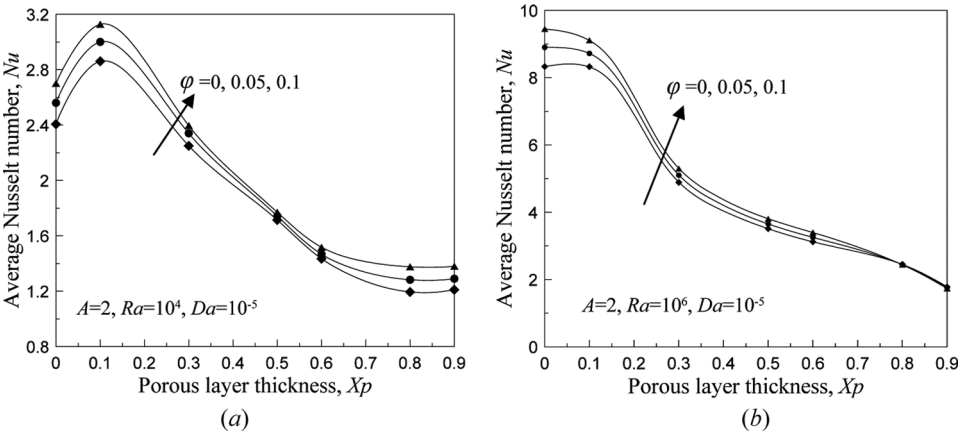

Figure 9. Variation of average Nusselt number with the porous layer thickness, (*a*) $\mathrm{Ra} = 10^4$, (*b*) $\mathrm{Ra} = 10^6$.

Figure 10 shows the effect of the Darcy number for $\mathrm{Ra} = 10^6$ and different other parameters. Generally, this figure indicates that the convection enhancement is started at $\mathrm{Da} = 10^{-5}$ and increases rapidly until $\mathrm{Da} = 10^{-2}$, provided that $Xp > 0.1$. This result was reported previously by several research papers, as in Goyeau and Gobin [21] and Gobin et al. [25] (for $N \leq 2$, where N is the ratio of solutal buoyancy to thermal buoyancy in their studies). The useless increase of Da from 10^{-7} to 10^{-5} which is reported in several previous works, can be treated, according

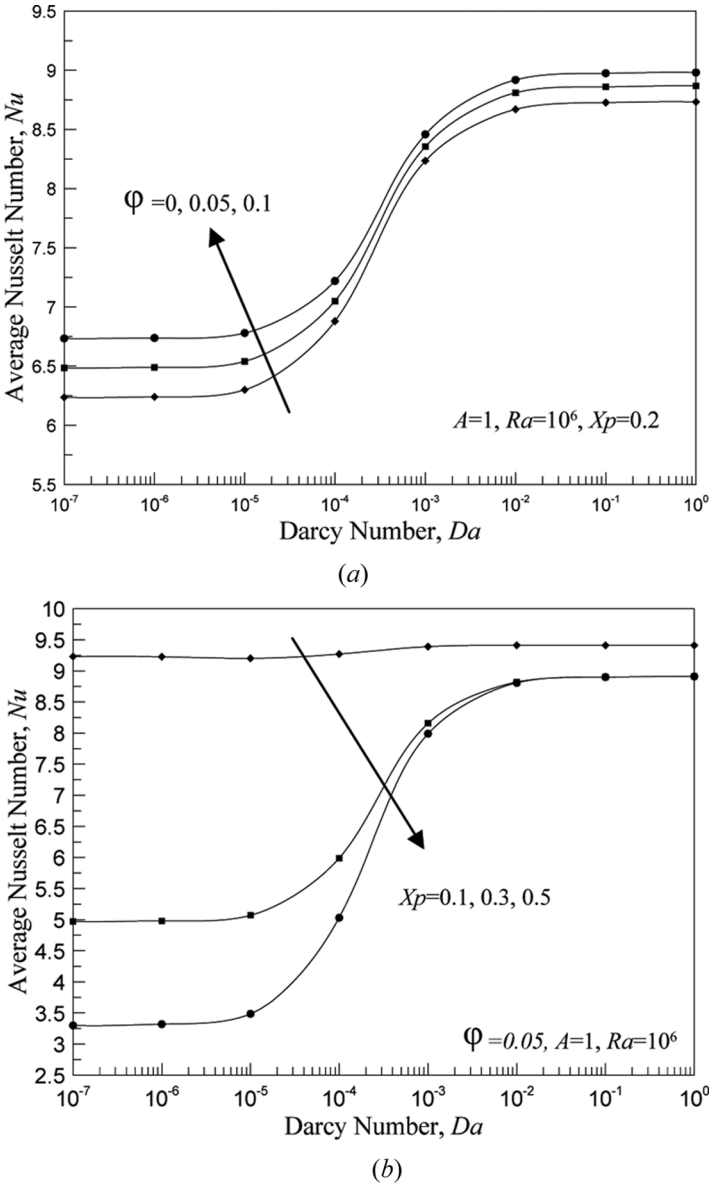

Figure 10. Variation of average Nusselt number with Da number, (*a*) φ effect, (*b*) Xp effect.

to the present study, by improving the thermal conductivity of the fluid confined in both layers. This fact is seen in Fig. 10a, where the increase of φ by 5% enhances Nu by 3.8% for $Da < 10^{-5}$, while for $Da > 10^{-2}$, the enhancement in Nu is about 1.9%. This is because of the large permeability medium which allows the flow to be freely accelerated and hence, competes the effect of the nanofluid action. Within the rapid Da increase range $10^{-4} \leq Da \leq 10^{-3}$, the addition of nanoparticles is of less significance. When the thickness of the porous layer is ≤ 0.1, the dimensionless permeability variation does not have a significant effect on the Nu, as shown in Figure 10*b*. As mentioned in several papers [24, 25], there is no significance for *Xp* when $Da \geq 10^{-2}$ i.e., the cavity seems to be composed of the nanofluid layer only. In the present study, Figure 10*b* emphasizes this fact, but not for all *Xp* values where at $Xp = 0.1$, say the critical porous layer thickness, there is no consistence of the curves at $Da = 1$. The reason of such discrepancy is attributed to that the present considered model of the thermal conductivity ratio of the porous layer to the nanofluid layer is not equal to unity as most research papers assumed. The explanation of Figure 9*a* is also useful to elucidate the very little effect of Da on Nu at this critical *Xp* value.

Figure 11 implies that regardless of the values of other parameters, Nu is an increasing function with Ra. The rate of increase of Nu with Ra is higher at a lower

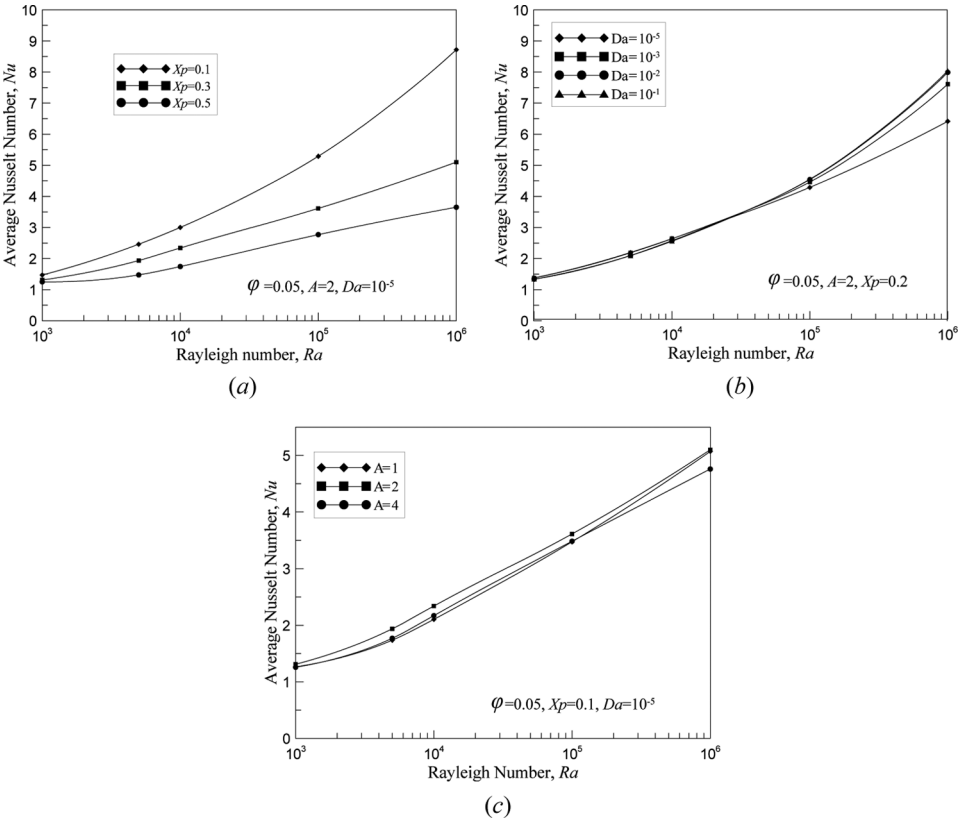

Figure 11. Variation of average Nusselt number with Ra number, (*a*) *Xp* effect, (*b*) Da effect, and (*c*) *A* effect.

thickness porous layer. This is because at higher Ra, the convection within the porous layer is frequently suppressed due to the dominance of the viscous and inertia forces. So that further increase in *Xp* leads to the increase of regions of suppressed convection. The overall cavity behaves as one layer cavity when $\mathrm{Ra} < 10^5$, as shown in Figure 11*b*. Beyond $\mathrm{Ra} = 10^5$, the permeability effect of the porous layer takes place where the lower Darcy number layer offers much resistance to natural convection.

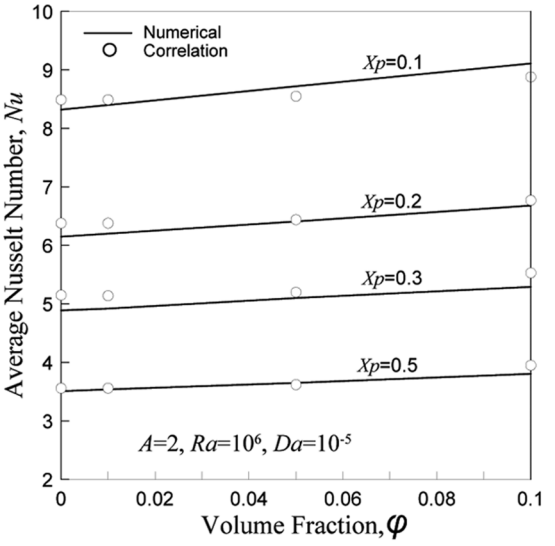

(*a*)

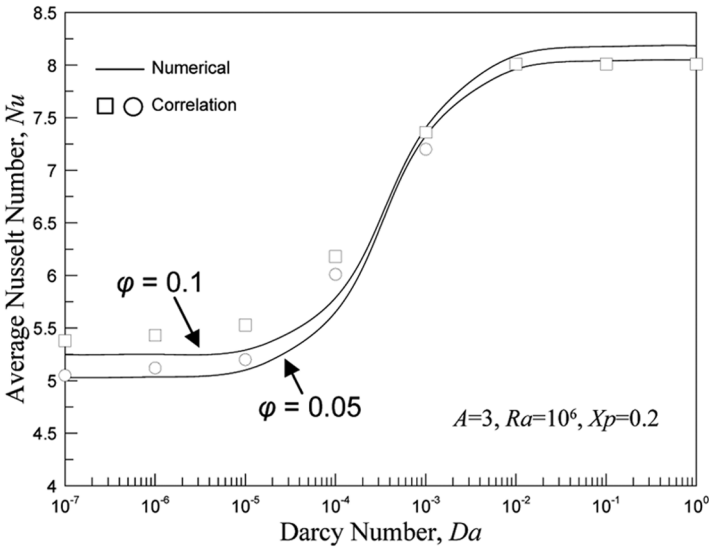

(*b*)

Figure 12. Test of the predicted correlations, (*a*) variation with φ, (*b*) variation with Da, square symbol for $\varphi = 0.05$ and circle symbol for $\varphi = 0.1$.

As previously mentioned, the increase in the aspect ratio A from 1 to 4 increases the space of cell rotation that leads to strengthening it and, hence, we expect increasing Nu as a result. At the same time, increasing A offers an increased resistance to the penetrated streamlines into the porous layer, so that when $A = 4$, the effect of the porous layer resistance overcomes the increase of Nu which in turn reduces Nu. What emphasizes this construction is the sudden increase of Nu at $A = 1$ beyond $\mathrm{Ra} = 10^5$ (Figure 6*b*). However, the unchanged single cell structure of streamlines with Ra (Figure 11*c*) is behind the little difference of Nu with A.

Eventually, the collected data of the average Nusselt number are utilized here in finding correlations for Nu with the studied parameters. From the insight made onto the collected numerical results, the effect of the aspect ratio A can safely be excluded from the correlations efforts as it has a negligible effect on Nu. The ranges of the other parameters are the same as those implemented in the numerical calculations. The obtained correlations are as follows.

$$\mathrm{Nu} = \begin{cases} 6.3195(1.0025 + \varphi^{2.789} - Xp^{0.0136})\mathrm{Ra}^{0.2599} + 0.044\,\mathrm{Da}^{1.3784} & \text{for } 10^{-7} \le \mathrm{Da} \le 10^{-5} \\ 5.8834(1.0329 + \varphi^{2.9329} - Xp^{0.0104})\mathrm{Ra}^{0.2388} + 1.237\,\mathrm{Da}^{1.4^{-5}} & \text{for } 10^{-4} \le \mathrm{Da} \le 10^{-3} \\ 4.147(1.0547 + \varphi^{2.9109} - Xp^{0.0023})\mathrm{Ra}^{0.254} + 5.2299\,\mathrm{Da}^{0.0098} & \text{for } 10^{-2} \le \mathrm{Da} \le 1 \end{cases}$$

The statistical effort is based on 95% confidence level and the values of correlation coefficient, R^2, between the numerical and correlated values are as follow: 0.9937 for $10^{-7} \le \mathrm{Da} \le 10^{-5}$, 0.9712 for $10^{-4} \le \mathrm{Da} \le 10^{-3}$ and 0.9964 for $10^{-2} \le \mathrm{Da} \le 1$. The clear features of these correlations is the reduction of Xp influence with increasing values of Da and the exponent of the solid volume fraction is the strongest among the other exponents. Figure 12 shows two sequences of Nu to assist and demonstrate the validity of the obtained correlations. However, we think that these correlations play an important role in the design of composed cavities filled with nanofluids.

5. CONCLUSIONS

Natural convection in differentially heated and partially porous cavity filled with a nanofluid was analyzed numerically based on the double–domain formulation. The main feature of this study was to determine if the conventional studied parameters in partially porous cavity like the permeability and the thickness of porous layer, Rayliegh number and the cavity aspect ratio are determined by the volume fraction of the nanoparticles or not. Therefore, combinations of five parameters effects were studied. The main derived conclusions from the results were as follows.

1. The use of nanofluid in partially porous cavities offered positive enhancement of convective heat transfer, and this effect manifested clearly in a low permeability porous layer.
2. The addition of nanoparticles was found to accelerate the flow throughout the cavity. The low Rayleigh number ($\mathrm{Ra} = 10^3$) was excluded from this trend.
3. The considered effective thermal conductivity of the porous layer showed that there was a critical porous layer thickness at which the convective heat transfer

was maximum. Hence, it was concluded that the material of the matrix forming the pores may play a significant role in such cavities.

4. The Nusselt number increased with Ra in a rapid form at lower porous layer thicknesses. The effect of the Darcy number manifested at higher values of the Rayleigh number ($Ra > 10^5$).
5. A partially porous cavity having its height twice that its width ($A = 2$), offered the best environment for convective heat transfer. However, the other two aspect ratios studied ($A = 1$ and 4) offered not noticeable discrepancy.

REFERENCES

1. G. S. Beavers and D. D. Joseph, Boundary Conditions at a Naturally Permeable Wall, *J. Fluid Mech.*, vol. 30, pp. 197–207, 1967.
2. T. W. Tong and E. Subramanian, Natural Convection in Rectangular Enclosures Partially Filled with a Porous Medium, *Int. J. Heat Fluid Flow*, vol. 7, pp. 3–10, 1986.
3. S. B. Sathe, W.-Q. Lin, and T. W. Tong, Natural Convection in Enclosures Containing Insulation with a Permeable Fluid–Porous Interface, *Int. J. Heat Fluid Flow*, vol. 9, pp. 389–395, 1988.
4. F. Chen and C. F. Chen, Convection in Superposed Fluid and Porous Layers, *J. Fluid Mech.*, vol. 234, pp. 97–119, 1992.
5. S. G. Kim and C. Y. Choi, Convective Heat Transfer in Porous and Overlying Fluid Layers Heated from Below, *Int. J. Heat Mass Transfer*, vol. 39, pp. 319–329, 1996.
6. A. K. Singh, T. Paul, and G. R. Thorpe, Natural Convection due to Heat and Mass Transfer in a Composite System, *Heat Mass Transfer*, vol. 35, pp. 39–48, 1999.
7. P. Zhao and C. F. Chen, Stability Analysis of Double–Diffusive Convection in Superposed Fluid and Porous Layers using a One-Equation Model, *Int. J. Heat Mass Transfer*, vol. 44, pp. 4625–4633, 2001.
8. J. J. Lopez and J. A. Tapia, A Study of Buoyancy Driven Flow in a Confined Fluid Overlying Porous Layer, *Int. J. Heat Mass Transfer*, vol. 44, pp. 4725–4736, 2001.
9. M. Carr and B. Straughan, Penetrative Convection in a Fluid Overlying a Porous Layer, *Adv. Water Resour.*, vol. 26, pp. 263–276, 2003.
10. B. A. Abu-Hijleh and M. A. Al-Nimr, The Effect of the Local Inertial Term on the Fluid Flow in Channels Partially Filled With Porous Material, *Int. J. Heat Mass Transfer*, vol. 44, pp. 1565–1572, 2001.
11. S. C. Hirata, B. Goyeau, D. Gobin, M. Carr, and R. M. Cotta, Linear Stability of Natural Convection in Superposed Fluid and Porous Layers: Influence of the Interfacial Modeling, *Int. J. Heat Mass Transfer*, vol. 50, pp. 1356–1367, 2007.
12. S. C. Hirata, B. Goyeau, and D. Gobin, Stability Analysis of Thermosolutal Natural Convection in a Partially Porous Medium, and *Proc. 5th European Thermal-Sciences Conf.*, The Netherlands, 2008.
13. S. C. Hirata, B. Goyeau, D. Gobin, M. Chandesris, and D. Jamet, Stability of Natural Convection in Superposed Fluid and Porous Layers: Equivalence of the One–and Two–Domain Approaches, *Int. J. Heat Mass Transfer*, vol. 52, pp. 533–536, 2009.
14. C. G. Aguilar-Madera, F. J. Valdés-Parada, B. Goyeau, and J. A. Ochoa-Tapia, One–Domain Approach for Heat Transfer between a Porous Medium and a Fluid, *Int. J. Heat Mass Transfer*, vol. 54, pp. 2089–2099, 2011.
15. A. Bagchi and F. A. Kulacki, Natural Convection in Fluid–Superposed Porous Layers Heated Locally from Below, *Int. J. Heat Mass Transfer*, vol. 54, pp. 3672–3682, 2011.

16. C. G. Aguilar-Madera, F. J. Valdés-Parada, B. Goyeau, and J. A. Ochoa-Tapia, Convective Heat Transfer in a Channel Partially Filled with a Porous Medium, *Int. J. Therm. Sci.*, vol. 50, pp. 1355–1368, 2011.
17. A. Bagchi and F. A. Kulacki, Experimental Study of Natural Convection in Fluid-Superposed Porous Layers Heated Locally from Below, *Int. J. Heat Mass Transfer*, vol. 55, pp. 1149–1153, 2012.
18. C. Beckermann, S. Ramadhyani, and R. Viskanta, Natural Convection Flow and Heat Transfer Between a Fluid Layer and a Porous Layer Inside a Rectangular Enclosure, *ASME J. Heat Transfer*, vol. 109, pp. 363–370, 1987.
19. P. H. Oosthuizen and J. T. Paul, Natural Convection in a Square Enclosure Partly Filled with Two Layers of Porous Material, *Trans. on Eng. Sci.*, vol. 12, pp. 63–72 WIT, 1996.
20. C. Beckermann and R. Viskanta, Natural Convection Solid/Liquid Phase Change in Porous Media, *Int. J. Heat Mass Transfer*, vol. 31, pp. 35–46, 1988.
21. B. Goyeau and D. Gobin, Heat Transfer by Thermosolutal Natural Convection in a Vertical Composite Fluid–Porous Cavity, *Int. Comm. Heat Mass Transfer*, vol. 26, pp. 1115–1126, 1999.
22. M. Mharzi, M. Daguenetb, and S. Daoud, Thermosolutal Natural Convection in a Vertically Layered Fluid-Porous Medium Heated from the Side, *Energ. Convers. Manageme.*, vol. 41, pp. 1065–1090, 2000.
23. J. F. Mercier, C. Weisman, M. Firdaouss, and P. Le Quére, Heat Transfer Associated to Natural Convection Flow in a Partly Porous Cavity, *ASME J. Heat Transfer*, vol. 124, pp. 130–143, 2002.
24. R. Bennacer, H. Beji, and A. A. Mohamad, Double Diffusive Convection in a Vertical Enclosure Inserted with Two Saturated Porous Layers Confining a Fluid Layer, *Int. J. Therm. Sci.*, vol. 42, pp. 141–151, 2003.
25. D. Gobin, B. Goyeau, and A. Neculae, Convective Heat and Solute Transfer in Partially Porous Cavities, *Int. J. Heat Mass Transfer*, vol. 48, pp. 1898–1908, 2005.
26. A. A. Merrikh and A. A. Mohamad, Non–Darcy Effects in Buoyancy Driven Flows in an Enclosure Filled with Vertically Layered Porous Media, *Int. J. Heat and Mass Transfer*, vol. 45, pp. 4305–4313, 2002.
27. M. S. Phanikumar and R. L. Mahajan, Non–Darcy Natural Convection in High Porosity Metal Foams, *Int. J. Heat and Mass Transfer*, vol. 45, pp. 3781–3793, 2002.
28. A. C. Baytas, A. F. Baytas, and D. B. Ingham, I. Pop, Double Diffusive Natural Convection in an Enclosure Filled with a Step Type Porous Layer: Non–Darcy Flow, *Int. J. Therm. Sci.*, vol. 48, pp. 665–673, 2009.
29. S. U. S. Choi, Enhancing Thermal Conductivity of Fluids with Nanoparticles, *ASME Fluids Eng. Div.*, vol. 231, pp. 99–105, 1995.
30. R. K. Tiwari and M. K. Das, Heat Transfer Augmentation in a Two-Sided Lid-Driven Differentially Heated Square Cavity Utilizing Nanofluids, *Int. J. Heat Mass Transfer*, vol. 50, pp. 2002–2018, 2007.
31. B. Ghasemi and S. M. Aminossadati, Natural Convection Heat Transfer in an Inclined Enclosure Filled with a Water-CuO Nanofluid, *Numer. Heat Transfer*, vol. 55, pp. 807–823, 2009.
32. E. Abu-Nada and H. F. Oztop, Numerical Analysis of Al_2O_3/Water Nanofluids Natural Convection in a Wavy Walled Cavity, *Numer. Heat Transfer*, vol. 59, pp. 403–419, 2011.
33. K. Khanafer, K. Vafai, and M. Lightstone, Buoyancy–Driven Heat Transfer Enhancement in a Two-Dimensional Enclosure Utilizing Nanofluids, *Int. J. Heat Mass Transfer*, vol. 46, pp. 3639–3653, 2003.
34. H. C. Brinkman, The Viscosity of Concentrated Suspensions and Solutions, *J. Chem. Phys.*, vol. 20, pp. 571–581, 1952.

35. M. Salari, M. M. Tabar, A. M. Tabar, and H. A. Danesh, Mixed Convection of Nanofluid Flows in a Square Lid-Driven Cavity Heated Partially From Both the Bottom and Side Walls, *Numer. Heat Transfer*, vol. 62, pp. 158–177, 2012.
36. A. H. Mahmoudi, M. Shahi, and F. Talebi, Entropy Generation due to Natural Convection in Partially Open Cavity with a Thin Heat Source Subjected to a Nanofluid, *Numer. Heat Transfer*, vol. 61, pp. 283–305, 2012.
37. B. Ghasemi, Magnetohydrodynamic Natural Convection of Nanofluids in U–Shaped Enclosure, *Numer. Heat Transfer*, vol. 63, pp. 473–487, 2013.
38. M. M. Rahman, M. M. Billah, M. Hasanuzzaman, R. Saidur, and N. A. Rahim, Heat Transfer Enhancement of Nanofluids in a Lid–Driven Square Enclosure, *Numer. Heat Transfer*, vol. 62, pp. 937–991, 2012.
39. R. Roslan, H. Saleh, and I. Hashim, Buoyancy–Driven Heat in Nanofluid–Filled Trapezoidal Enclosure with Variable Thermal Conductivity and Viscosity, *Numer. Heat Transfer*, vol. 60, pp. 867–882, 2011.
40. E. Weinan and Jian-Guo Liu, Vorticity Boundary Condition and Related Issues for Finite Difference Schemes, *J. Comput. Phys.*, vol. 124, pp. 368–382, 1996.
41. G. de Vahl Davis, Natural Convection of Air in a Square Cavity, A Benchmark Numerical Solution, *Int. J. Numer. Methods Fluids*, vol. 3, pp. 249–264, 1962.
42. G. Lauriat and V. Prasad, Non–Darcian Effects on Natural Convection in a Vertical Porous Enclosure, *Int. J. Heat Mass Transfer*, vol. 32, pp. 2135–2148, 1989.
43. S. Das and R. K. Sahoo, Effect of Darcy, Fluid Rayleigh and Heat Generation Parameters on Natural Convection in a Porous Square Enclosure: A Brinkman-Extended Darcy Model, *Int. Comm. Heat Mass Transfer*, vol. 26, pp. 569–578, 1999.
44. H. Sajjadi, M. Gorji, G. H. R. Kefayati, and D. D. Ganji, Lattice Boltzmann Simulation of Turbulent Natural Convection in Tall Enclosure using Cu/Water Nanofluid, *Numer. Heat Transfer*, vol. 62, pp. 512–530, 2012.
45. A. J. Chamkha and M. A. Ismael, Conjugate Heat Transfer in a Porous Cavity Filled with Nanofluids and Heated by a Triangular Thick Wall, *Int. J. Therm. Sci.*, vol. 67, pp. 135–151, 2012.